

# Discovery of a compact hierarchical triple main-sequence star system while searching for binary stars with compact objects

Ataru TANIKAWA,<sup>1,\*</sup> Akito TAJITSU,<sup>2</sup> Satoshi HONDA,<sup>3</sup> Hiroyuki MAEHARA,<sup>2</sup> Bunei SATO,<sup>4</sup> Kento MASUDA,<sup>5</sup> Masashi OMIYA,<sup>6</sup> Hideyuki IZUMIURA,<sup>2</sup>

<sup>1</sup>Center for Information Science, Fukui Prefectural University, 4-1-1 Matsuoka Kenjojima, Eiheiji-cho, Fukui 910-1195, Japan

<sup>2</sup>Subaru Telescope Okayama Branch, National Astronomical Observatory of Japan, 3037-5, Honjou, Kamogata, Asakuchi, Okayama 719-0232, Japan

<sup>3</sup>Nishi-Harima Astronomical Observatory, Center for Astronomy, University of Hyogo, Sayo, Hyogo 679-5313, Japan

<sup>4</sup>Department of Earth and Planetary Sciences, Institute of Science Tokyo, 2-12-1 Ookayama, Meguro-ku, Tokyo 152-8551, Japan

<sup>5</sup>Department of Earth and Space Science, Graduate School of Science, Osaka University, 1-1 Machikaneyama-cho, Toyonaka, Osaka 560-0043, Japan

<sup>6</sup>Astrobiology Center, 2-21-1 Osawa, Mitaka, Tokyo 181-8588, Japan

\*E-mail: tanik@g.fpu.ac.jp

ORCID: 0000-0002-8461-5517, 0000-0001-8813-9338, 0000-0001-6653-8741, 0000-0003-0332-0811, 0000-0001-8033-5633, 0000-0003-1298-9699, 0000-0002-5051-6027

## Abstract

We have discovered a compact hierarchical triple main-sequence star system, which is cataloged as Gaia DR3 1010268155897156864 or TIC 21502513. Hereafter, we call it “G1010”. G1010 consists of a primary (the most massive) star and inner binary that orbit each other. The primary star is a  $0.85^{+0.03}_{-0.03} M_{\odot}$  main-sequence (MS) star, and the inner binary components are  $0.63^{+0.02}_{-0.02}$  and  $0.61^{+0.02}_{-0.02} M_{\odot}$  MS stars. The outer and inner orbital periods are  $277.2^{+1.6}_{-1.3}$  and  $\sim 18.26$  days, respectively. G1010 is categorized as a single-lined spectroscopic binary, and its orbital solution indicates that G1010 possibly accompanies a massive compact object, such as a neutron star or massive white dwarf. In order to confirm the presence of a massive compact object, we have performed several-times low signal-to-ratio (SNR) and one-time high SNR spectroscopic observations, and determined the outer orbital parameters. Moreover, we have deeply analyzed the high SNR spectroscopic data, and found that G1010 accompanies not a massive compact object, but an inner binary. We have investigated G1010’s light curve in Transiting Exoplanet Survey Satellite (TESS), and concluded that the inner binary is actually an eclipsing binary, not included in TESS Eclipsing Binary Stars. We have obtained the inner orbital parameters from the TESS light curve. G1010 is similar to compact hierarchical triple star systems previously discovered by eclipse timing variation analysis. Our discovery has shown that such triple star systems can be discovered by combination of low- and high-SNR spectroscopic observations with the help of Gaia DR3 and the upcoming Gaia DR4/DR5.

**Keywords:** binaries: spectroscopic — binaries: eclipsing — binaries: close

## 1 Introduction

White dwarfs (WDs), neutron stars (NSs), and black holes (BHs) are compact objects that stars leave behind after they exhaust their nuclear fuels. Isolated compact objects simply cools and fades over time. However, compact objects often merge, and their mergers may cause fascinating astronomical transients: BH-BH and BH-NS mergers as gravitational wave sources (Abbott et al. 2023), NS-NS mergers as multi-messenger sources (Abbott et al. 2017), and WD-WD mergers as one of the most promising progenitors for type Ia supernovae (Iben & Tutukov 1984; Webbink 1984). This motivates astronomers to search for binary stars with compact objects, hereafter compact binaries.

Very recently, compact binaries have been discovered from Gaia Data Release 3 (DR3: Gaia Collaboration et al. 2023a) with spectroscopic follow-up observations, such as Gaia BHs (El-Badry et al. 2023b; 2023a; Tanikawa et al. 2023; Chakrabarti et al. 2023; Gaia Collaboration et al. 2024), Gaia NSs (El-Badry 2024b; 2024),

detached WD binaries (Yamaguchi et al. 2024b; 2024a; Zhao et al. 2024), and a binary consisting of hot subdwarf star and compact object (Geier et al. 2023). These compact binaries have orbital periods of  $\sim 10^2 - 10^3$  days, which are much longer than compact binaries previously discovered by X-ray and radio observations (El-Badry 2024a).

However, there remains a possibility that compact objects in these binaries are indeed two objects. In other words, these compact binaries could be triple star systems. Hereafter, we call these compact objects and compact binaries “compact object candidates” and “compact binary candidates”, respectively. The compact object candidates of Gaia BH2 and BH3 may be inner double BHs instead of single BHs, while Nagarajan et al. (2024) have ruled out the possibility that Gaia BH1 contains inner double BHs. Note that Tanikawa et al. (2025) have pointed out the formation rate of such triple systems is not rare if they are formed in open clusters. The possibility that the compact object candidates of Gaia NSs are inner double WDs has not yet been excluded (El-

Badry 2024b; El-Badry et al. 2024). Detached WD binaries may not be binaries with WDs and main-sequence (MS) stars, but triple MS stars (Yamaguchi et al. 2024b; 2024a). One reason why there remain these possibilities is that these compact binary candidates have long periods. They can be stable even if they contain inner binaries. Note that many compact binaries with orbital periods of  $\lesssim 10$  days have been also discovered recently (Mazeh et al. 2022; Zheng et al. 2022; 2023; Shenar et al. 2022; Li et al. 2022; Yuan et al. 2022; Yi et al. 2022; Qi et al. 2023; Ding et al. 2024; Rowan et al. 2024; Zhang et al. 2024; Tucker et al. 2025; Zhu et al. 2025 Shiraishi et al. 2025). They are more unlikely to contain inner binaries because of their short orbital periods.

In this paper, we report our survey and discovery of a triple star system during the search for compact binaries with orbital periods of  $10^2 - 10^3$  days. Because we search for such compact binaries, our triple star system has outer orbital periods of  $10^2 - 10^3$  days. Such triple star systems are categorized into “compact” triple star systems because of their short orbital periods. Previous studies have discovered similar triple star systems via eclipsing time variation analysis (Steffen et al. 2011; Gies et al. 2012; 2015; Rappaport et al. 2013; 2022; 2024; Borkovits et al. 2013; 2015; 2016; 2020; 2025b; 2025a; Lee et al. 2013; 2014; 2015; Tokovinin 2014a; 2014b; Conroy et al. 2014; Zasche et al. 2015; Baran et al. 2015; Hajdu et al. 2019; 2022; Mitnyan et al. 2020; 2024; Gaulme et al. 2022; Yenawine et al. 2022; Eisner et al. 2022; Moharana et al. 2023; 2024; Czavalinga et al. 2023; Yang et al. 2023; Kostov et al. 2024; Rocha et al. 2025). Our triple star system is not included in their discoveries. It is not found in a list of quadruple star candidates (Kostov et al. 2026). Moreover, we discover it by only spectroscopic observations. Indeed, after the discovery, we recognize that its inner binary is an eclipsing binary from the light curve of Transiting Exoplanet Survey Satellite (TESS). The delay in our recognition results from the fact that the triple star system is not included in catalogs of eclipsing binaries, such as TESS Eclipsing Binary Stars (Prša et al. 2022).

The remainder of this paper is structured as follows. In section 2, we organize our terminology, and show the parameters of our triple star system in advance. In section 3, we describe how to select our targets from Gaia DR3. In section 4, we introduce the instruments we use for our follow-up observations. In section 5, we present our analysis to determine the outer orbit of our triple star system. In sections 6 and 7, we show how to detect the inner binary, and determine its orbital parameters. In section 8, we compare our triple star system with triple star systems discovered by previous surveys. In section 9, we make conclusions in this paper.

## 2 Terminology and notations

We organize our terminology in this paper. Figure 1 shows what stars are called “primary”, “secondary”, and “tertiary” stars. We name them in order of decreasing mass and optical luminosity. Note that our naming rule might be different from the naming rule of researchers who discover triple star systems via eclipsing time variation analysis. They name components of a triple star system in order from the inside out. In other words, they call our primary star “tertiary star”. This difference comes from the fact that we first recognize the presence of the primary star, while they finally recognize it.

We call the pair of the secondary and tertiary stars “inner binary”, or “faint companion” of the primary star. We use the term of the faint companion, when we analyze the radial velocity (RV) variation of the primary star (see sections 3 and 5). In the analysis,

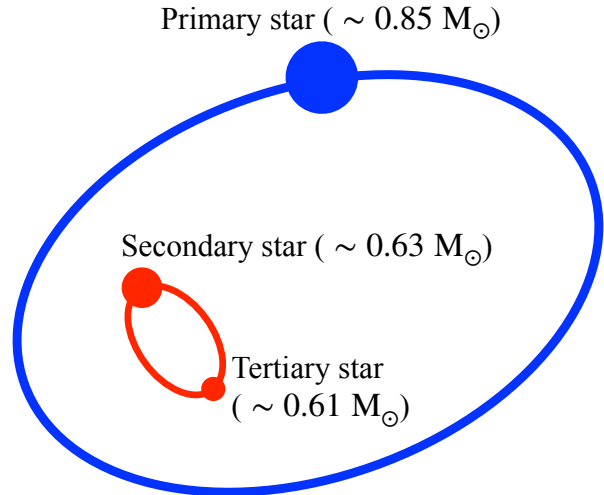


**Fig. 1.** Primary, secondary, and tertiary stars of our triple stars.

we just regard it as a single object. We call the orbit of the inner binary “inner orbit”, and the relative motion between the primary star and inner binary “outer orbit”.

We summarize the parameters of Gaia DR3 1010268155897156864 or TIC 21502513 in Table 1. We abbreviate it to G1010. We divide these parameters into four: the parameters provided by Gaia DR3, the outer orbit parameters derived by our RV variation analysis, the parameters of the three stars obtained from high signal-to-noise-ratio (SNR) spectroscopy, and the inner orbit parameters estimated from their eclipses. We attach the subscripts “out” and “in” to parameters related to the outer and inner orbits, respectively. We also attach the subscripts “1”, “2”, and “3” to parameters related to the primary, secondary, and tertiary stars, respectively.

## 3 Selection of targets

Although we report the discovery of one triple star system in this paper, we primarily search for detached compact binaries from the table “`nss_two_body_orbit`” in Gaia DR3 (Gaia Collaboration et al. 2023a). Here, we describe our method to narrow down compact binary candidates. The table `nss_two_body_orbit` contains about 200,000 objects with binary orbital solutions. They are categorized into “Orbital”, “SB1”, and “AstroSpectroSB1” by a data type “`nss_solution_type`”, where the binary orbital solution of an object with “Orbital”, “SB1”, and “AstroSpectroSB1” is based on astrometric data, spectroscopic data, and both astrometric and spectroscopic data, respectively. We select our targets, put the following constraints on these objects.

1. The apparent magnitude of an object is less than 13 mag in the G band because of the limiting magnitude of the instruments we use.
2. The declination of an object is more than  $-20$  degree because of our observing sites.
3. The primary star of an object is G- or K-type star. Such a star has many absorption lines in the optical band.
4. The primary star of an object has a faint companion whose mass

**Table 1.** Summary of Gaia DR3 1010268155897156864 or TIC 21502513.

Names	
Abbreviation	G1010
Gaia source ID	1010268155897156864
TESS Identity Catalog	21502513
Parameters from Gaia DR3	
NSS solution type	SB1
Right Ascension (RA)	8 <sup>h</sup> 51 <sup>m</sup> 50 <sup>s</sup> 60
Declination (Dec)	44°55'11.9"
Apparent magnitude in G band (G) [mag]	12.67
Renormalized Unit Weight Error (RUWE)	4.58
Parallax ( $\varpi$ ) [mas]	2.30 $\pm$ 0.25*
Outer orbit from RV variation	
RV semi-amplitude ( $K_1$ ) [km/s]	25.36 <sup>+0.69</sup> <sub>-0.66</sub>
Orbital period ( $P_{\text{out}}$ ) [day]	277.2 <sup>+1.6</sup> <sub>-1.3</sub>
Orbital eccentricity ( $e_{\text{out}}$ )	0.230 <sup>+0.019</sup> <sub>-0.018</sub>
Argument of periastron ( $\omega_1$ ) [deg]	166.2 <sup>+6.0</sup> <sub>-6.2</sub>
Periastron passage ( $t_{\text{p,out},2016}$ ) [day]	119.7 <sup>+10.1</sup> <sub>-18.9</sub>
Periastron passage ( $t_{\text{p,out},2023.5}$ ) [day]	-122.0 <sup>+3.2</sup> <sub>-2.9</sub>
Center-of-mass velocity ( $\gamma$ ) [km/s]	-4.25 <sup>+0.34</sup> <sub>-0.33</sub>
Mass function ( $f_m$ ) [ $M_{\odot}$ ]	0.431 <sup>+0.033</sup> <sub>-0.031</sub>
SB3 spectral and isochrone fittings	
Age ( $t_{\text{age}}$ ) [Gyr]	12.17 <sup>+1.16</sup> <sub>-1.87</sub>
Initial metallicity ([Fe/H] <sub>init</sub> )	-0.33 <sup>+0.09</sup> <sub>-0.09</sub>
Effective temperature ( $T_{\text{eff},1}$ ) [K]	5869 <sup>+65</sup> <sub>-60</sub>
Mass ( $m_1$ ) [ $M_{\odot}$ ]	0.85 <sup>+0.03</sup> <sub>-0.03</sub>
Radius ( $R_1$ ) [ $R_{\odot}$ ]	1.10 <sup>+0.08</sup> <sub>-0.07</sub>
Effective temperature ( $T_{\text{eff},2}$ ) [K]	4584 <sup>+75</sup> <sub>-71</sub>
Mass ( $m_2$ ) [ $M_{\odot}$ ]	0.63 <sup>+0.02</sup> <sub>-0.02</sub>
Radius ( $R_2$ ) [ $R_{\odot}$ ]	0.63 <sup>+0.02</sup> <sub>-0.02</sub>
Effective temperature ( $T_{\text{eff},3}$ ) [K]	4454 <sup>+70</sup> <sub>-67</sub>
Mass ( $m_3$ ) [ $M_{\odot}$ ]	0.61 <sup>+0.02</sup> <sub>-0.02</sub>
Radius ( $R_3$ ) [ $R_{\odot}$ ]	0.61 <sup>+0.02</sup> <sub>-0.02</sub>
Center-of-mass velocity ( $\gamma$ ) [km/s]	-4.93 <sup>+0.18</sup> <sub>-0.16</sub>
Modified mass function ( $f_m \sin^{-3} i$ ) [ $M_{\odot}$ ]	0.432 <sup>+0.016</sup> <sub>-0.017</sub>
Inner orbit from eclipses	
Orbital period ( $P_{\text{in}}$ ) [day]	18.3 <sup>†</sup>

\* The uncertainty of parallax is inflated, based on the formula proposed by El-Badry (2025). The inflation factor is 3.34 for G1010.

† We do not show the uncertainty of the inner orbital period, because we do not rigorously analyze eclipse timing.

is larger than, or equal to  $1.35 M_{\odot}$  (described in detail below).

5. The primary star of an object does not outshine its faint companion if the faint companion is a single star in its zero-age (ZA) main-sequence (MS) phase (described in detail below).

In the constraint 4, we estimate the faint companion mass for Orbital and AstroSpectroSB1, or the minimum mass of the faint companion for SB1. For this purpose, we need the primary star mass in addition to the binary orbital solution. We obtain the primary star mass as follows. We construct a table consisting of ZAMS star masses and their G-band absolute magnitude, based on the MESA Isochrones & Stellar Tracks (MIST) model (Paxton et al. 2011; 2013; 2015; Choi et al. 2016; Dotter 2016), where we adopt the solar metallicity. We derive the primary star mass, giving the table its G-band absolute magnitude as input. Indeed, we do not estimate the primary star mass accurately. The primary star does not always have the solar metallicity, and is not a ZAMS star. Moreover, we do not take into account the interstellar extinction of the primary star. We use the estimated mass just as a simple indicator in order to deal with a large number of objects. If the G-band luminosity of a primary star is fixed, the primary star tends

to have small masses as its age increases, and its metallicity decreases. In other words, we would overestimate the primary star masses overall, which effectively means we overestimate the faint companion masses. Consequently, our selected targets can have faint companions of  $< 1.35 M_{\odot}$ .

The constraint 5 enables us to avoid an object which contains a faint companion difficult to identify as either compact object or non-degenerate star like a MS star. For example, even if the faint companion mass is  $2 M_{\odot}$ , we cannot identify if it is a NS or just a MS star, when the primary star is much more luminous than a  $2 M_{\odot}$  MS star. For this constraint, we estimate the G-band absolute magnitude of a faint companion, referring to the table constructed above, given that the faint companion is a ZAMS star. When its G-band absolute magnitude is more than that of the primary star, we remove the object from our targets.

We obtain a target list containing  $\sim 50$  objects as detached compact binary candidates. From our target list, we focus on one candidate, which is identified as a triple star system later. We name it G1010 after the initial character of “Gaia” and the first four digits of its Gaia source ID. G1010 is the first to have its identity determined in our target list. We perform follow-up observations for several objects, however have not yet found out what they are.

## 4 Follow-up observations

### 4.1 Gunma Astronomical Observatory Echelle Spectrograph for Radial Velocity

We obtain 17 spectra with the Gunma Astronomical Observatory Echelle Spectrograph for Radial Velocity (GAOES-RV, Sato et al. 2024) on the 3.8-m Seimei telescope at the Okayama observatory from the second half of 2023 to the first half of 2025 (programmes 23B-N-CN02, 24A-N-CN03, 24A-K-0024, 24B-N-CN04, 24B-K-0013, 25A-N-CN18, and 25A-K-0023). The wavelength coverage is 516 – 593 nm. The spectral resolution is  $R \sim 65000$ . We use the ThAr lamp as a wavelength calibration light source, not using the iodine ( $I_2$ ) cell. This is because we do not need an accuracy of  $\sim 10$  m/s, and the apparent magnitudes of our targets are close to the limiting magnitude of GAOES-RV. Exposure times range from 900 to 1800 s for each spectrum, depending on weather conditions. The SNR per pixel is typically  $\sim 20$ .

### 4.2 Medium And Low-dispersion Long-slit Spectrograph

We obtain 9 spectra with the Medium And Low-dispersion Long-slit Spectrograph (MALLS) on the 2-m NAYUTA Telescope at the Nishi-Harima Astronomical Observatory from the second half of 2023 to the first half of 2025. We adopt the 1.2'-width slit and the 1800 l/mm grating. This settings achieve a wavelength coverage 40 nm centered on the wavelength range of  $H_{\alpha}$ . The spectral resolution is  $R \sim 7500$ . Exposure times are 3000 s. The SNR per pixel is typically  $\sim 20$ .

### 4.3 High Dispersion Spectrograph

We obtain 1 spectra with the High Dispersion Spectrograph (HDS) on the 8.2-m Subaru telescope at the NAOJ Hawaii Observatory. The settings are as follows. We choose the standard spectrograph setup “StdYb” in which the wavelength regions are 414 – 535 nm and 559 – 681 nm. The slit width we use is 0.4", which provides a resolving power of  $R \sim 90\,000$ . Exposure times are 1500 s for

**Table 2.** RVs of the primary star in G1010.

Julian epoch year	RV [km/s]	Instrument
2023.8502	$-19.3 \pm 0.8$	GAOES-RV
2023.9325	$-34.7 \pm 1.0$	GAOES-RV
2023.9352	$-35.8 \pm 1.2$	GAOES-RV
2023.9920	$-29.8 \pm 1.3$	GAOES-RV
2024.0109	$-26.6 \pm 1.5$	GAOES-RV
2024.0275	$-22.7 \pm 1.6$	GAOES-RV
2024.0301	$-22.2 \pm 1.3$	GAOES-RV
2024.0414	$-22.9 \pm 2.4$	MALLS
2024.0797	$-8.5 \pm 5.3$	MALLS
2024.0876	$-10.0 \pm 1.3$	GAOES-RV
2024.0989	$-8.9 \pm 4.1$	MALLS
2024.1287	$-2.5 \pm 0.9$	GAOES-RV
2024.1509	$-1.1 \pm 4.9$	MALLS
2024.1890	$+5.8 \pm 1.0$	GAOES-RV
2024.2112	$+11.9 \pm 2.4$	MALLS
2024.2331	$+14.3 \pm 6.8$	MALLS
2024.2604	$+17.0 \pm 3.3$	MALLS
2024.2960	$+15.3 \pm 3.6$	MALLS
2024.8468	$-9.1 \pm 1.6$	GAOES-RV
2024.8495	$-9.2 \pm 1.0$	GAOES-RV
2024.9066	$-0.1 \pm 5.7$	MALLS
2024.9669	$+9.0 \pm 1.5$	GAOES-RV
2025.0246	$+12.7 \pm 1.1$	GAOES-RV
2025.1014	$+14.5 \pm 1.2$	GAOES-RV
2025.2615	$+4.8 \pm 0.4$	HDS

each spectrum. The SNR per pixel is typically  $\sim 200$ .

## 5 Outer orbit from radial velocity variation

We summarize the RVs of the primary star in G1010 in Table 2. We obtain a RV from each spectrum as follows. For GAOES-RV data, we identify 60 – 70 absorption lines between 517 and 533 nm in each spectrum. We fit the absorption lines with a Gaussian, compare their median values with the Atomic Spectra Database (ASD) provided by National Institute of Standards and Technology<sup>1</sup>, and derive a RV for each absorption line. We take the arithmetic mean of all these RVs, and regard it as the representative value at the epoch. We regard the standard error of all these RVs as the error of the representative value of the RV. For the HDS data, we adopt the same method to obtain the RV, except that we find 100 absorption lines between 517 and 534 nm in the HDS spectrum. For MALLS data, we spot 5 absorption lines in each spectrum. We obtain RVs in the same way as for the case of GAOES-RV, except that we refer to the atomic line list in Kurucz & Bell (1995). The atomic line database is different from those referred in the case of GAOES-RV and HDS, however the resulting systematic error in RVs should be  $\lesssim 0.1$  km/s. It does not affect our results.

We assume that the RVs of the primary star follows the Keplerian motion. We obtain its orbital elements, using a Markov Chain Mote Carlo (MCMC) method. Its free parameters we adopt are the RV semi-amplitude of the primary star ( $K_1$ ), outer orbital period ( $P_{\text{out}}$ ), outer orbital eccentricity ( $e_{\text{out}}$ ), argument of periastron of the primary star ( $\omega_1$ ), outer periastron time ( $t_{\text{p,out},2023.5}$ ), and center-of-mass RV of the system ( $\gamma$ ). Note that the reference epoch is 2023.5 in the Julian year. We set uniform priors on all parameters in the following ranges:

- $[0.4(\text{max RV}_i - \text{min RV}_i), 0.6(\text{max RV}_i - \text{min RV}_i)]$  for  $K_1$ , where  $\text{RV}_i$  is a RV we measure at each epoch.
- $[0.8P_{\text{Gaia}}, 1.2P_{\text{Gaia}}]$  for  $P_{\text{out}}$ , where  $P_{\text{Gaia}}$  is an orbital period

indicated in Gaia DR3.

- No constraint, or  $[0, 1]$  for  $e_{\text{out}}$ .
- No constraint for  $\omega_1$ .
- No constraint for  $t_{\text{p,out},2023.5}$ .
- $[\text{min RV}_i, \text{max RV}_i]$  for  $\gamma$ .

The likelihood function can be expressed as

$$\log L = -\frac{1}{2} \sum_i \frac{(\text{RV}_{\text{pred},i} - \text{RV}_i)^2}{\sigma_{\text{RV},i}^2}, \quad (1)$$

where  $\text{RV}_{\text{pred},i}$  is the predicted RV at the same epoch as  $\text{RV}_i$ , and  $\sigma_{\text{RV},i}$  is the error associated with the  $\text{RV}_i$  measurement. The actual values of  $\text{RV}_i$  and  $\sigma_{\text{RV},i}$  are shown in Table 2. We implement the above MCMC method with the help of emcee (Foreman-Mackey et al. 2013).

In Figure 2, we draw our best-fitting and  $1\sigma$ -confidence models for the RVs of the primary star in G1010. We also summarize their orbital elements in Table 3 (see also Table 1). For comparison, we also show RV variations (Figure 2) and orbital elements (Table 3) derived from Gaia DR3. We show the outer periastron time,  $t_{\text{p,out},2016}$  and  $t_{\text{p,out},2023.5}$ , setting the reference epoch to 2016 and 2023.5 in the Julian year, respectively. We find that the outer orbital elements of G1010 are consistent between Gaia DR3's and our models within  $1\sigma$  confidence. Although Gaia DR3's and our RV variations look different in Figure 2, it is only a phase difference. Since the orbital elements derived from Gaia DR3 are based on observational data during 2014 – 2017, a small error in the periastron time increases during 2023.5 – 2025.5 as seen in  $t_{\text{p,out},2016}$  and  $t_{\text{p,out},2023.5}$  of Table 3.

For reference, we indicate spectroscopic mass functions ( $f_m$ ) in Table 3. The spectroscopic mass functions can be given by

$$f_m = \frac{(m_2 + m_3)^3}{(m_1 + m_2 + m_3)^2} \sin^3 i_{\text{out}} \\ = 1 \text{ M}_\odot \left( \frac{K_1}{29.8 \text{ km/s}} \right)^3 \left( \frac{P_{\text{out}}}{1 \text{ year}} \right) (1 - e_{\text{out}}^2)^{3/2}, \quad (2)$$

where  $i_{\text{out}}$  is the inclination angle between our line of sight, and the direction of the orbital angular momentum of a binary star. We find that our spectroscopic mass function ( $0.431^{+0.033}_{-0.031} \text{ M}_\odot$ ) is consistent with that derived from Gaia DR3 ( $0.485^{+0.096}_{-0.070} \text{ M}_\odot$ ) within  $1\sigma$ .

## 6 Identification of the Inner Binary with HDS Spectroscopy

To assess the possibility that the faint companion is itself an unresolved inner binary, we analyze the six reddest HDS orders, where a putative inner binary would contribute a larger fractional flux relative to the primary star (Section 6.1). An initial one-star (SB1) model leaves two additional sets of absorption lines visible in the cross-correlation function (CCF), prompting us to adopt a three-star (SB3) model that successfully reproduces all three sets of lines. Using the atmospheric parameters and flux ratios inferred from the SB3 spectral fit, we perform an isochrone analysis to estimate the masses of the three components and the systemic velocity of the triple system (Section 6.2). These spectroscopically inferred properties are consistent with those independently derived from the outer orbit (Section 5). Together, these results strongly support the interpretation that the system is a hierarchical triple consisting of the primary star and an inner binary. The code used for the analysis presented in this section and the HDS spectrum is available on GitHub.<sup>2</sup>

<sup>1</sup> <https://www.nist.gov/pml/atomic-spectra-database>

<sup>2</sup> <https://github.com/kemasuda/g1010/tree/main>

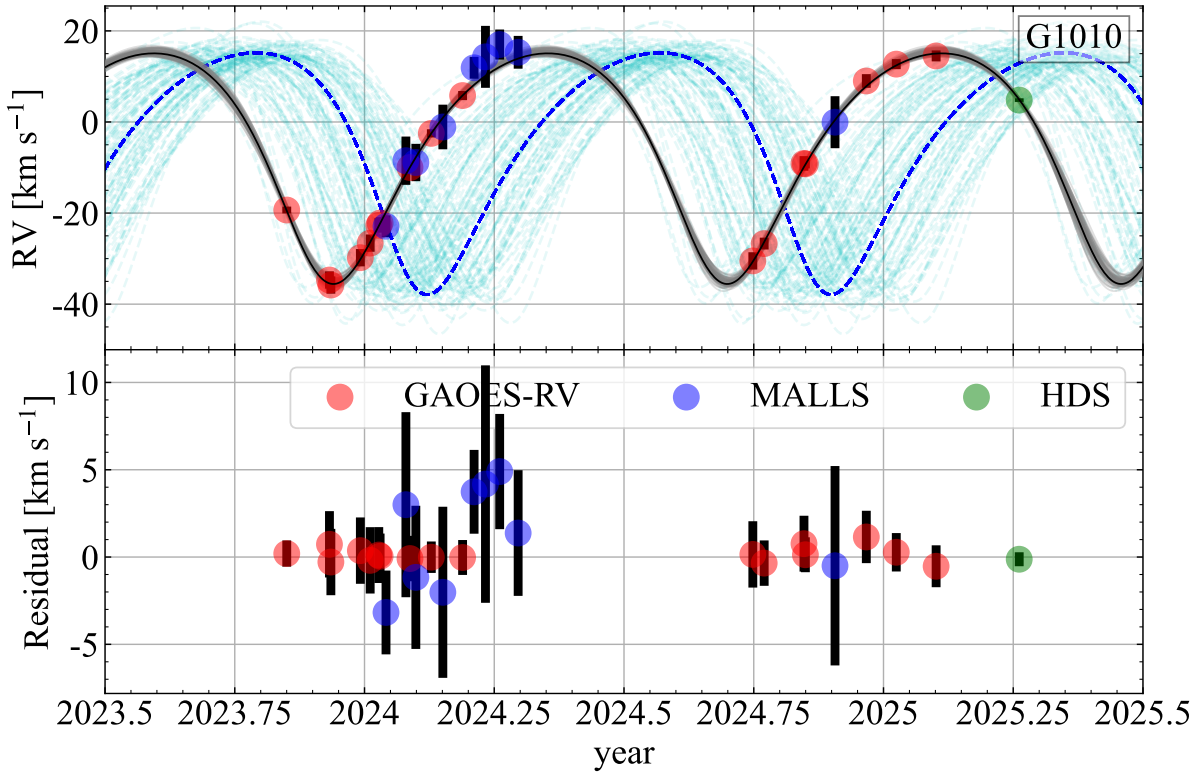


**Fig. 2.** RV variation of the primary star of G1010. In the top panel, our best-fitting model is indicated by the solid thick curve. The  $1\sigma$ -confidence models are drawn by the solid thin curves. The dashed thick and thin curves show the best-fitting and  $1\sigma$ -confidence models provided by Gaia DR3. In the bottom panel, RV residuals from our best-fitting model are shown.

**Table 3.** Comparison between orbital parameters of this work and Gaia DR3 for G1010.

	$K_1$ [km/s]	$P_{\text{out}}$ [day]	$e_{\text{out}}$	$\omega_1$ [deg]	$t_{\text{p,out},2016}$ [day]	$t_{\text{p,out},2023.5}$ [day]	$\gamma$ [km/s]	$f_m$ [ $M_\odot$ ]
This work	$25.36^{+0.69}_{-0.66}$	$277.2^{+1.6}_{-1.3}$	$0.230^{+0.019}_{-0.018}$	$166.2^{+6.0}_{-6.2}$	$119.7^{+10.1}_{-18.9}$	$-122.0^{+3.2}_{-2.9}$	$-4.25^{+0.34}_{-0.33}$	$0.431^{+0.033}_{-0.031}$
Gaia DR3	$26.43^{+1.87}_{-1.44}$	$284.4^{+2.6}_{-2.9}$	$0.275^{+0.051}_{-0.054}$	$157.7^{+20.9}_{-20.0}$	$115.3^{+14.2}_{-14.0}$	$-64.7^{+36.6}_{-32.9}$	$-4.73^{+1.02}_{-0.91}$	$0.485^{+0.096}_{-0.070}$

## 6.1 Modeling of the HDS Spectrum

We fit the HDS spectrum with synthetic models using `jaxspec`.<sup>3</sup> The code interpolates the synthetic grid, Doppler-shifts it according to the RV  $v$ , and convolves it with a line-broadening kernel that includes the projected rotational velocity  $v \sin i$ , macroturbulence  $\zeta$ , quadratic limb-darkening coefficients ( $q_a, q_b$ ) following Kipping (2013), and a Gaussian instrumental profile corresponding to  $R = 90,000$ . Further details of the implementation can be found in Tomoyoshi et al. (2024). Unlike in that paper, here we employ the synthetic grid of Coelho et al. (2005), computed as a function of effective temperature  $T_{\text{eff}}$ , surface gravity  $\log g$ , metallicity [Fe/H], and  $\alpha$ -enhancement [ $\alpha$ /Fe]. This grid was generated with the PFANT LTE spectral-synthesis code using ATLAS9 model atmospheres (Castelli & Kurucz 2003) and adopting the solar abundances of Grevesse & Sauval (1998).

We first perform a SB1 fit to the six HDS orders following the procedure described in Tomoyoshi et al. (2024), finding an RV of  $\sim 4.7$  km/s, consistent with the outer-orbit analysis (Section 5). We then compute the residual spectrum and cross-correlated it

with a solar-like template. The resulting CCF exhibits two additional peaks at  $\sim -48.5$  km/s and  $\sim 25.4$  km/s, both with nearly equal amplitudes (Figure 3). These two sets of lines are also visually apparent in the middle panels of Figure 4, where the primary star model from the SB3 fit (see below) is subtracted from the data. This pattern strongly suggests the presence of a relatively close, nearly equal-mass binary, which we refer to as secondary and tertiary stars in the following.

Motivated by this, we refit the same spectral orders with a SB3 model, in which the normalized flux model  $F_{\text{model}}$  is represented as the sum of three Doppler-shifted and broadened synthetic spectra:

$$F_{\text{model}}(\lambda) = [(1 - f_2 - f_3)F_1(\lambda) + f_2F_2(\lambda) + f_3F_3(\lambda)] \times \left( c_a + c_b \frac{\lambda - \lambda_{\text{mean}}}{\lambda_{\text{max}} - \lambda_{\text{min}}} \right), \quad (3)$$

where  $\lambda_{\text{mean}}$ ,  $\lambda_{\text{max}}$ , and  $\lambda_{\text{min}}$  are the mean, maximum, and minimum wavelengths within each order. The parameters  $c_a$  and  $c_b$  account for the normalization and slope in the data. The flux ratios  $f_2$  and  $f_3$  were assumed to be constant with wavelength over the limited range of the orders analyzed. The model was computed

<sup>3</sup> <https://github.com/kemasuda/jaxspec>

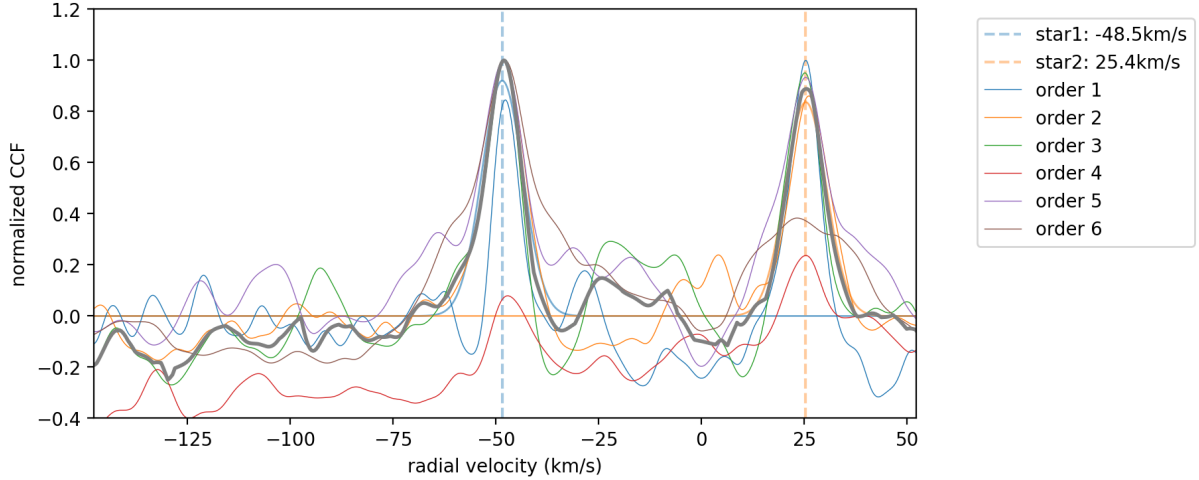


**Fig. 3.** Normalized CCFs between the solar-like template and the residual of the SB1 fit described in Section 6.1. Different colors represent different orders. The thick gray line shows the median of the six CCFs.

for each order labeled by  $k$ , for which we adopt the following Gaussian-process likelihood:

$$\ln \mathcal{L}^{(k)} = -\frac{1}{2}(F_{\text{obs}}^{(k)} - F_{\text{model}}^{(k)})^T \Sigma^{-1} (F_{\text{obs}}^{(k)} - F_{\text{model}}^{(k)}) - \frac{1}{2} \ln |2\pi\Sigma|, \quad (4)$$

where the covariance matrix between pixels  $i$  and  $j$  is

$$\Sigma_{ij} = (\sigma_i^2 + s^2) \delta_{ij} + \rho^2 \left( 1 + \frac{\sqrt{3}|\lambda_i - \lambda_j|}{l} \right) \exp \left( -\frac{\sqrt{3}|\lambda_i - \lambda_j|}{l} \right), \quad (5)$$

with  $\sigma_i$  fixed at  $5 \times 10^{-3}$  based on the typical SNR,  $s$  accounting for any excess white noise,  $\rho$  the covariance amplitude, and  $l$  the correlation length. The total log-likelihood is  $\ln \mathcal{L} = \sum_k \ln \mathcal{L}^{(k)}$ . We first minimize  $-\ln \mathcal{L}$  using stochastic variational inference (SVI), and then sample from the posterior using the No-U-Turn Sampler (Hoffman & Gelman 2011) as implemented in NumPyro (Bingham et al. 2018; Phan et al. 2019) adopting the priors as listed in Table 4. We run four independent chains, obtained 500–5000 effective samples for all parameters, and checked adequate mixing using standard convergence diagnostics, finding split Gelman–Rubin statistics  $\hat{R} < 1.01$  (Gelman et al. 2014).

The resulting constraints are summarized in Table 4. The superscripts (1)–(6) indicate parameters independently fitted for each order. The metallicity and  $\alpha$ -enhancement are assumed to be common among all three stars, and the noise parameters were assumed to be common among the six orders. The mean model is compared with the data in Figure 4. The middle panel in each set shows the residuals relative to the primary star alone, and the bottom panel shows the residuals relative to the full SB3 model. The two sets of residual features producing the CCF peaks (Figure 3) match the spectra of two  $\sim 4500$ K stars, each contributing  $\lesssim 10\%$  of the total flux.

## 6.2 Three-star Isochrone Fitting

Given the constraints on the atmospheric parameters of the three stars, as well as their flux ratios, we next perform an isochrone fitting to the unresolved SB3 system to infer the physical parameters of the components. We use the `jaxstar` code described in Masuda (2022),<sup>4</sup> which interpolates the MIST isochrones (Paxton

et al. 2011; Paxton et al. 2013; Paxton et al. 2015; Choi et al. 2016; Dotter 2016) to compute the relevant stellar properties as a function of the initial bulk metallicity  $[\text{Fe}/\text{H}]_{\text{init}}$ , age  $t_{\text{age}}$ , and the equivalent evolutionary phase  $\text{eep}$  (Dotter 2016). The latter essentially corresponds to the stellar mass  $m$  given  $[\text{Fe}/\text{H}]_{\text{init}}$  and  $t_{\text{age}}$ .

The model parameters are the  $\text{eep}$  values of the three stars; a common  $t_{\text{age}}$  and  $[\text{Fe}/\text{H}]_{\text{init}}$  for the system; and the distance  $d$ . The fitted observables are the extinction-corrected  $K_s$  magnitude (using  $A(K_s) = 0.3026$  and  $E(B-V) = 0.107$ ), the Gaia DR3 parallax  $\varpi$ , the effective temperatures  $T_{\text{eff}}$  of the three stars, a common photospheric  $[\text{Fe}/\text{H}]$ , and the flux ratios  $f_2$  and  $f_3$  in the HDS wavelength range spanning 638–681 nm. Note that we obtain  $E(B-V)$ , adopting the extinction factor  $R_V = 3.1$  (Cardelli et al. 1989), and the V-band extinction  $A_V$  from the 3D dust map of Lallement et al. (2022) and Vergely et al. (2022) through GTOMO<sup>5</sup>. The model  $K_s$  magnitude is taken to be the sum of the contributions from the three stars; the common  $[\text{Fe}/\text{H}]$  is modeled as the mean value of the three stars; and  $f_2$  and  $f_3$  are computed with `jaxspec` and the grid of Coelho et al. (2005) as the ratio of the mean fluxes in the above range multiplied by the squared radius ratio. The likelihood for the observables is assumed to be an independent Gaussian for each quantity as described in Masuda (2022), where the uncertainties for  $T_{\text{eff}}$  and  $[\text{Fe}/\text{H}]$  are inflated to 100 K and 0.1 dex, respectively. The posterior samples are obtained using the same sampler as in the SB3 spectral fit. We run four independent chains, obtain 1000–3000 effective samples, and assessed chain mixing with  $\hat{R} < 1.01$  for all parameters.

The results are summarized in Table 5, together with the adopted priors. The masses of the three stars are inferred to be about  $0.85$ ,  $0.63$ , and  $0.61 M_{\odot}$ . Using the posterior samples for these parameters, together with the radial velocities from the spectral fit (Section 6.1), we compute  $f_m \sin^{-3} i_{\text{iso}} = (m_2 + m_3)^3 / (m_1 + m_2 + m_3)^2$  for the outer orbit and the center-of-mass velocity

$$\gamma_{\text{iso}} = \frac{m_1 v_1 + m_2 v_2 + m_3 v_3}{m_1 + m_2 + m_3} \quad (6)$$

of the three-body system. The resulting  $f_m \sin^{-3} i_{\text{iso}} =$

<sup>4</sup> <https://github.com/kemasuda/jaxstar>

<sup>5</sup> <https://explore-platform.eu/sda/g-tomo>

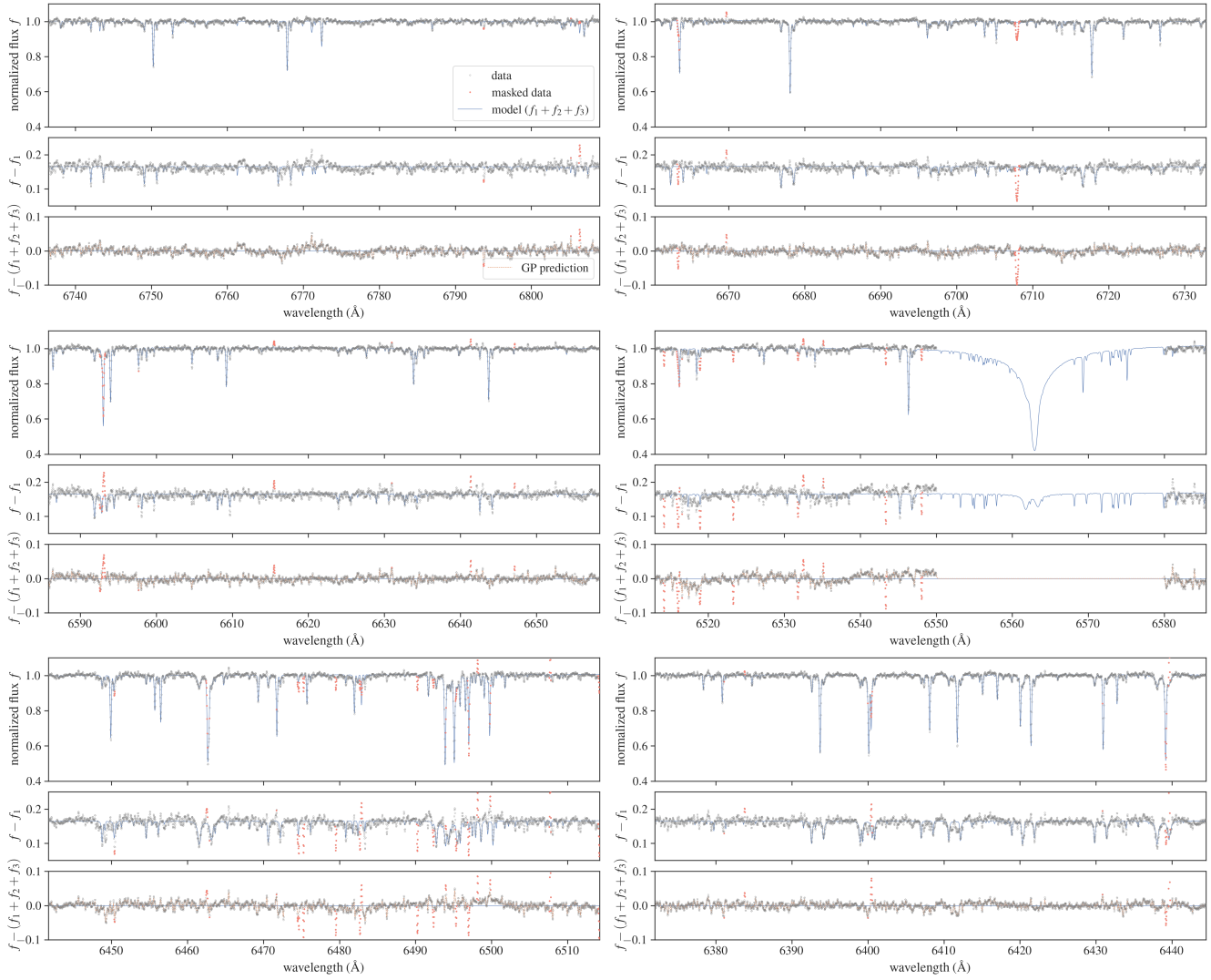


**Fig. 4.** The reddest six orders of the HDS spectrum (gray circles) and the spectral model (blue lines) from Section 6.1. Each three-panel set shows the result for one order. In each set, the top panel compares the synthesized SB3 spectrum with the normalized HDS flux, while the middle and bottom panels show the residuals obtained by subtracting the synthesized SB1 and SB3 spectra from the normalized HDS flux, respectively. In the bottom panels, the orange dotted lines indicate the mean prediction of the Gaussian-process component, and the filled red circles mark data points that are identified as outliers and excluded from the fit.

$0.432^{+0.016}_{-0.017} M_{\odot}$  (68%) agrees with the value from the RV orbit (Table 3) for  $\sin i \approx 1$ , and  $\gamma_{\text{iso}} = -4.93^{+0.18}_{-0.16} \text{ km/s}$  is consistent with the RV-based value within the  $2\sigma$  level. We emphasize that these values are obtained entirely from the single HDS spectrum and are therefore essentially independent of the orbital analysis in Section 5. The agreement strongly indicates that the RV motion of the primary star is caused by the two fainter stars identified in the HDS spectrum — that is, the system is a G+(K+K) hierarchical triple.

We synthesize the spectrum of G1010 using stellar parameters obtained from the isochrone fitting, and compare the spectra with the broad-band spectral energy distributions (SED) of G1010. For the spectral synthesis, we use the `pystellib` code<sup>6</sup> with the BaSeL library (Lejeune et al. 1997; 1998), adopting parameters obtained from the three-star isochrone fitting. We use the interstellar reddening  $E(B - V) = 0.107$  as described above. We con-

struct the broad-band SED of G1010 as follows. We adopt WISE W<sub>1</sub>W<sub>2</sub>W<sub>3</sub> photometry (Wright et al. 2010), 2MASS JHK photometry (Skrutskie et al. 2006), u Sloan Digital Sky Survey (SDSS) photometry (Padmanabhan et al. 2008) and GALEX NUV photometry (Martin et al. 2005), retrieving these data from VizieR (Ochsenbein et al. 2000). We synthesize griz SDSS photometry (Padmanabhan et al. 2008), filtering Gaia XP spectra (Gaia Collaboration et al. 2023b) with `pyphot`, a tool for computing photometry from spectra (Fouesneau 2025). As seen Figure 5, the synthesized spectrum is consistent with the the broad-band SED. The residuals of the photometry lie within about 0.1 mag.

## 7 Further Evidence for the Inner Binary from TESS

G1010 corresponds to TIC 21502513 in the TESS mission (Ricker et al. 2015) and is observed in sectors 21 and 47. Figures 6 and

<sup>6</sup> <https://github.com/mfouesneau/pystellib>

**Table 4.** Priors and Posterior Constraints from the Spectral Analysis

Parameter	Posterior	Prior
<b>(Atmospheric Parameters)</b>		
$T_{\text{eff},1}$ [K]	$5749^{+14}_{-14}$	$\mathcal{U}(3500, 7000)$
$T_{\text{eff},2}$ [K]	$4565^{+58}_{-67}$	$\mathcal{U}(3500, 7000)$
$T_{\text{eff},3}$ [K]	$4575^{+76}_{-85}$	$\mathcal{U}(3500, 7000)$
$\log g_1$	$4.382^{+0.040}_{-0.043}$	$\mathcal{U}(3, 5)$
$\log g_2$	$4.33^{+0.15}_{-0.14}$	$\mathcal{U}(3, 5)$
$\log g_3$	$4.30^{+0.24}_{-0.21}$	$\mathcal{U}(3, 5)$
[Fe/H]	$-0.447^{+0.011}_{-0.010}$	$\mathcal{U}(-1, 0.5)$
$[\alpha/\text{Fe}]$	$0.0050^{+0.0070}_{-0.0036}$	$\mathcal{U}(0, 0.4)$
$(v \sin i)_1$ [km/s]	$2.20^{+0.14}_{-0.13}$	$\mathcal{U}(0, 15)$
$(v \sin i)_2$ [km/s]	$2.89^{+0.37}_{-0.44}$	$\mathcal{U}(0, 15)$
$(v \sin i)_3$ [km/s]	$2.37^{+0.56}_{-0.82}$	$\mathcal{U}(0, 15)$
$\zeta_1$ [km/s]	$3.948^{+0.021}_{-0.022}$	$\mathcal{N}(\zeta_{\text{emp}}(T_{\text{eff}}), 1)$
$\zeta_2$ [km/s]	$2.13^{+0.09}_{-0.10}$	$\mathcal{N}(\zeta_{\text{emp}}(T_{\text{eff}}), 1)$
$\zeta_3$ [km/s]	$2.14^{+0.12}_{-0.13}$	$\mathcal{N}(\zeta_{\text{emp}}(T_{\text{eff}}), 1)$
$q_{a,1}$	$0.44^{+0.36}_{-0.31}$	$\mathcal{U}(0, 1)$
$q_{a,2}$	$0.51^{+0.33}_{-0.35}$	$\mathcal{U}(0, 1)$
$q_{a,3}$	$0.51^{+0.33}_{-0.35}$	$\mathcal{U}(0, 1)$
$q_{b,1}$	$0.43^{+0.36}_{-0.30}$	$\mathcal{U}(0, 1)$
$q_{b,2}$	$0.51^{+0.34}_{-0.36}$	$\mathcal{U}(0, 1)$
$q_{b,3}$	$0.51^{+0.33}_{-0.34}$	$\mathcal{U}(0, 1)$
<b>(Flux Ratios)</b>		
$f_2$	$0.0923^{+0.0032}_{-0.0031}$	$\mathcal{U}(0, 0.25)$
$f_3$	$0.0727^{+0.0032}_{-0.0031}$	$\mathcal{U}(0, 0.25)$
<b>(Radial Velocities)</b>		
$RV_1^{(1)}$ [km/s]	$4.833^{+0.057}_{-0.062}$	$\mathcal{U}(-0.21, 9.78)$
$RV_1^{(2)}$ [km/s]	$4.920^{+0.046}_{-0.049}$	$\mathcal{U}(-0.21, 9.78)$
$RV_1^{(3)}$ [km/s]	$4.707^{+0.049}_{-0.048}$	$\mathcal{U}(-0.21, 9.78)$
$RV_1^{(4)}$ [km/s]	$4.783^{+0.072}_{-0.073}$	$\mathcal{U}(-0.21, 9.78)$
$RV_1^{(5)}$ [km/s]	$4.735^{+0.032}_{-0.032}$	$\mathcal{U}(-0.21, 9.78)$
$RV_1^{(6)}$ [km/s]	$4.702^{+0.029}_{-0.030}$	$\mathcal{U}(-0.21, 9.78)$
<b>(Noise Parameters)</b>		
$\ln \rho$	$-4.643^{+0.014}_{-0.014}$	$\mathcal{U}(-5, -0.5)$
$\ln l$ [Å]	$-2.168^{+0.018}_{-0.017}$	$\mathcal{U}(-5, 2)$
$\ln s$	$-9.67^{+0.35}_{-0.23}$	$\mathcal{U}(-10, -3)$
<b>(Flux Normalization and Slope)</b>		
$c_a^{(1)}$	$1.00268^{+0.00064}_{-0.00060}$	$\mathcal{U}(0.8, 1.2)$
$c_a^{(2)}$	$1.00280^{+0.00061}_{-0.00064}$	$\mathcal{U}(0.8, 1.2)$
$c_a^{(3)}$	$1.00317^{+0.00060}_{-0.00062}$	$\mathcal{U}(0.8, 1.2)$
$c_a^{(4)}$	$1.01009^{+0.00093}_{-0.00091}$	$\mathcal{U}(0.8, 1.2)$
$c_a^{(5)}$	$1.00387^{+0.00064}_{-0.00062}$	$\mathcal{U}(0.8, 1.2)$
$c_a^{(6)}$	$1.00414^{+0.00062}_{-0.00059}$	$\mathcal{U}(0.8, 1.2)$
$c_b^{(1)}$	$0.0002^{+0.0020}_{-0.0020}$	$\mathcal{U}(-0.2, 0.2)$
$c_b^{(2)}$	$-0.0066^{+0.0021}_{-0.0020}$	$\mathcal{U}(-0.2, 0.2)$
$c_b^{(3)}$	$-0.0049^{+0.0020}_{-0.0020}$	$\mathcal{U}(-0.2, 0.2)$
$c_b^{(4)}$	$0.0257^{+0.0028}_{-0.0029}$	$\mathcal{U}(-0.2, 0.2)$
$c_b^{(5)}$	$0.0063^{+0.0021}_{-0.0021}$	$\mathcal{U}(-0.2, 0.2)$
$c_b^{(6)}$	$0.0009^{+0.0021}_{-0.0021}$	$\mathcal{U}(-0.2, 0.2)$

Note — Values listed here report the medians and 68% equal-tail intervals of the marginal posteriors.  $\mathcal{U}(a, b)$  denotes the uniform probability density function between  $a$  and  $b$ .  $\mathcal{N}(\mu, \sigma)$  denotes the normal distribution with mean  $\mu$  and standard deviation  $\sigma$ . The  $\zeta_{\text{emp}}(T_{\text{eff}})$  was computed using the empirical relation (equation 1) in Valenti & Fischer (2005) where we have corrected the sign of the linear term.

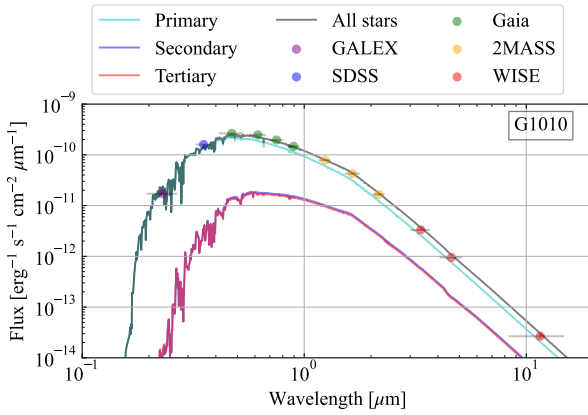


**Fig. 5.** SED of G1010. We construct these SEDs, retrieving WISE  $W_1 W_2 W_3$ , 2MASS JHK, u SDSS, and GALEX NUV photometry from VizieR, and calculating griz SDSS photometry, filtering Gaia XP spectra with pyphot. We synthesize several spectra by means of the pyphot code.

7 displays the full light curve and the zoomed-in views of the eclipses for this source, respectively. We identify three eclipses in sector 21 and two in sector 47. The characteristics of these eclipse events are as follows: the first three eclipses (sector 21) exhibit similar durations and depths, as do the final two (sector 47). However, the eclipses in sector 21 are notably longer and deeper than those in sector 47. The measured time intervals between successive events – the 1st and 2nd, 2nd and 3rd, and 4th and 5th eclipses – are approximately 9.0, 9.3, and 8.9 days, respectively.

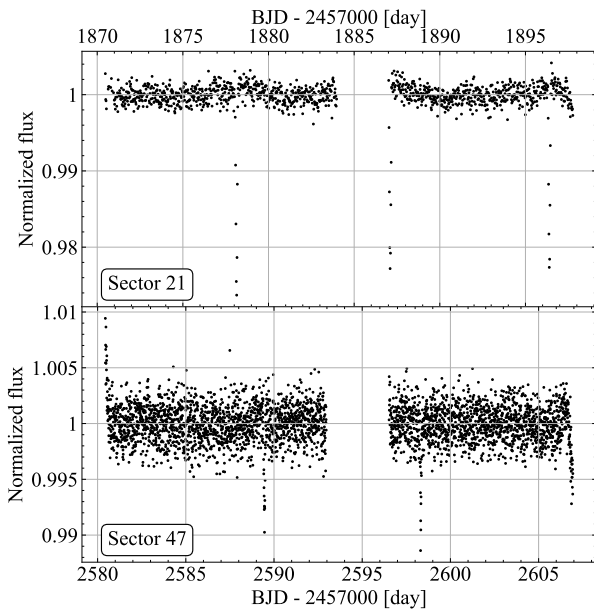
We infer that the three eclipses in sector 21 correspond to the primary and secondary eclipses of the inner binary of G1010. We also suggest that these eclipses are diluted by the flux of the primary star. This interpretation is supported by the following three points, which are consistent with our findings in Section 6. First, the three eclipses exhibit similar durations and depths. This observation aligns with our isochrone fitting results (Section 6.2), which indicate that the inner binary consists of two stars with nearly identical masses and radii.

Second, the time interval between the 1st and 3rd eclipses ( $\sim 18.3$  days) is expected to correspond to the orbital period of the inner binary. Based on this, the average relative velocity of the inner binary components can be estimated as:

**Table 5.** Priors and Posterior Constraints from the Isochrone Analysis

Parameter	Posterior	Prior
distance [kpc]	$0.465^{+0.029}_{-0.028}$	$\Gamma(3, 1.58)$
age $t_{\text{age}}$ [Gyr]	$12.2^{+1.2}_{-1.9}$	$\mathcal{U}(0.1, 13.8)$
EEP <sub>1</sub>	$420^{+10}_{-12}$	$\mathcal{U}(0, 500)$
EEP <sub>2</sub>	$341.4^{+3.0}_{-4.6}$	$\mathcal{U}(0, 500)$
EEP <sub>3</sub>	$338.4^{+3.0}_{-4.7}$	$\mathcal{U}(0, 500)$
[Fe/H] <sub>init</sub>	$-0.334^{+0.087}_{-0.086}$	$\mathcal{U}(-1, 0.5)$
$\varpi$ [mas]	$2.15^{+0.14}_{-0.13}$	*
$T_{\text{eff},1}$	$5869^{+65}_{-60}$	*
$T_{\text{eff},2}$	$4585^{+75}_{-71}$	*
$T_{\text{eff},3}$	$4454^{+70}_{-67}$	*
$f_2$	$0.0918^{+0.0029}_{-0.0030}$	*
$f_3$	$0.0736^{+0.0029}_{-0.0028}$	*
[Fe/H] <sub>1</sub>	$-0.450^{+0.100}_{-0.098}$	
[Fe/H] <sub>2</sub>	$-0.385^{+0.092}_{-0.089}$	
[Fe/H] <sub>3</sub>	$-0.380^{+0.091}_{-0.089}$	
mean [Fe/H]	$-0.405^{+0.094}_{-0.092}$	*
$K_{s,1}$ [mag]	$11.415^{+0.031}_{-0.031}$	
$K_{s,2}$ [mag]	$12.955^{+0.057}_{-0.053}$	
$K_{s,3}$ [mag]	$13.078^{+0.056}_{-0.051}$	
total $K$ [mag]	$11.006^{+0.021}_{-0.021}$	*
$m_1$ [ $M_{\odot}$ ]	$0.851^{+0.030}_{-0.025}$	
$m_2$ [ $M_{\odot}$ ]	$0.628^{+0.020}_{-0.020}$	
$m_3$ [ $M_{\odot}$ ]	$0.606^{+0.020}_{-0.020}$	
$R_1$ [ $R_{\odot}$ ]	$1.099^{+0.082}_{-0.073}$	
$R_2$ [ $R_{\odot}$ ]	$0.625^{+0.019}_{-0.020}$	
$R_3$ [ $R_{\odot}$ ]	$0.605^{+0.019}_{-0.022}$	
$f_m \sin^3 i_{\text{iso}}$ [ $M_{\odot}$ ]	$0.432^{+0.016}_{-0.017}$	
$\gamma_{\text{iso}}$ [km/s]	$-4.93^{+0.18}_{-0.16}$	

Note — Values listed here report the medians and 68% equal-tail intervals of the marginal posteriors. Parameters with \* in the prior column are the fitted observables; see Section 6.2.

**Fig. 6.** Normalized light curves for G1010 (TIC 21502513) from TESS sectors 21 and 47. Nominal values are plotted.

$$v \sim 87 \left( \frac{m_2 + m_3}{1.24 M_{\odot}} \right)^{1/3} \left( \frac{P_{\text{in}}}{18.3 \text{ day}} \right)^{-1} [\text{km/s}], \quad (7)$$

where  $P_{\text{in}}$  denotes the inner orbital period. This value is consistent with the relative velocity of  $\sim 73.9$  km/s derived from our SB3 spectral fit (Section 6.1). The fact that the 2nd eclipse does not occur exactly halfway between the 1st and 3rd eclipses suggests that the inner binary possesses a small orbital eccentricity ( $\sim 0.01$ ).

Third, the observed durations of these eclipses are approximately 0.1 days (see Figure 7). For comparison, we can estimate the expected durations using the relative velocity derived above and the radii of the secondary and tertiary stars obtained from the isochrone fitting in Section 6.2. The duration  $D$  is given by:

$$D \sim 0.11 \left( \frac{R}{0.6 R_{\odot}} \right) \left( \frac{v}{87 \text{ km/s}} \right)^{-1} [\text{day}], \quad (8)$$

where  $R$  denotes the radius of the secondary or tertiary star. This calculated duration is in excellent agreement with the observations shown in Figure 7.

The time interval between the 4th and 5th eclipses (8.9 days) deviates significantly from those of the 1st and 2nd (9.0 days) and the 2nd and 3rd (9.3 days) eclipses. Furthermore, the eclipse depths also differ between sectors 21 and 47. We speculate that these discrepancies can be attributed to three-body effects: specifically, apsidal precession may account for the varying time intervals, while nodal precession explains the changes in eclipse depth. The timescale for the inner orbit of G1010 to precess by  $180^{\circ}$  can be estimated as follows:

$$t_{3\text{body}} \sim 6.7 \times 10^3 \left( \frac{m_2 + m_3}{1.24 M_{\odot}} \right) \left( \frac{m_1}{0.85 M_{\odot}} \right)^{-1} \times \left( \frac{a_{\text{in}}}{0.147 \text{ au}} \right)^{-3} \left( \frac{a_{\text{out}}}{1.06 \text{ au}} \right)^3 \left( \frac{P_{\text{in}}}{18.3 \text{ day}} \right) [\text{day}], \quad (9)$$

assuming a circular inner orbit and coplanarity between the inner and outer orbits (i.e., mutual inclination of zero). Given that the time interval between sectors 21 and 47 is 710 days – a value comparable to  $t_{3\text{body}}$  – it is plausible that the distinct eclipse features observed across these sectors are driven by three-body dynamical effects.

## 8 Comparison with previous discoveries

We compare our triple system G1010 with previous surveys. Tokovinin (2018) have published the Multiple Star Catalog that includes not only compact triple star systems but also resolved triple star systems. However, G1010 is not in the catalog. Many studies have searched for triple star systems via eclipse time variations from Kepler binaries (Steffen et al. 2011; Gies et al. 2012; 2015; Rappaport et al. 2013; Borkovits et al. 2013 2015; 2016; 2025b; Lee et al. 2013; 2014; 2015; Conroy et al. 2014; Zasche et al. 2015; Baran et al. 2015; Gaulme et al. 2022; Yenawine et al. 2022; Moharana et al. 2023). Hajdu et al. (2019; 2022) have made a list of triple star system candidates, based on eclipse time variation analysis of OGLE-IV eclipsing binaries. G1010 is not included in triple star systems discovered by these surveys, since G1010 is outside of the Kepler mission star field and the OGLE-IV field. Many triple star systems have been discovered via eclipse time variations from TESS (Borkovits et al. 2020; 2025a; Mitnyan et al. 2020; 2024; Rappaport et al. 2022; 2024; Yang et al. 2023; Moharana et al. 2024; Kostov et al. 2024; Eisner et al. 2022). However, these studies have not found G1010.

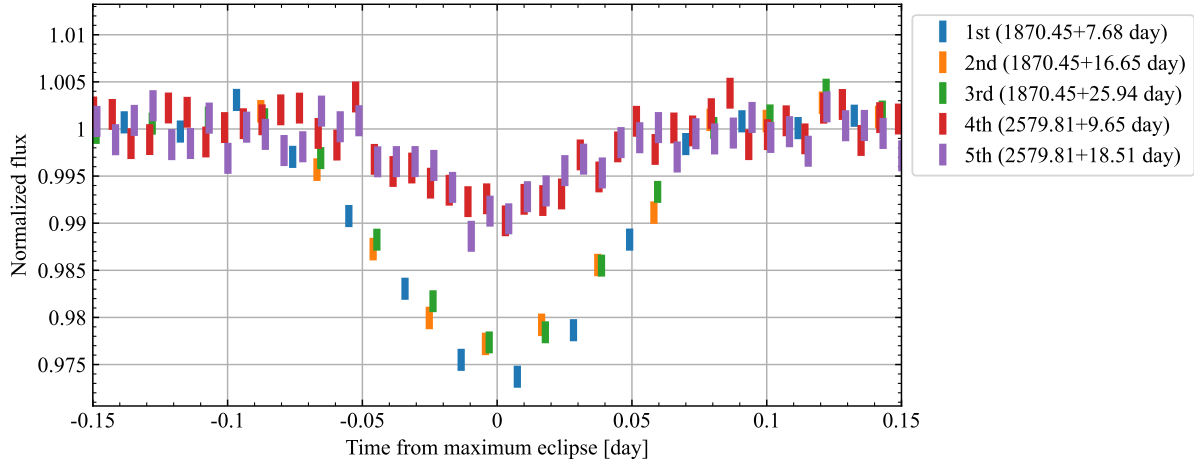


**Fig. 7.** Normalized light curves for G1010 (TIC 21502513) from TESS sectors 21 and 47. Sector 21 includes the 1st, 2nd, and 3rd eclipses, while sector 47 covers the 4th and 5th. For each event, the time axis is shifted to center the maximum eclipse at zero. The specific shift amounts, expressed in BJD – 2457000 [days], are detailed in the legend. Error bars are plotted.

Czavalinga et al. (2023) have provided a list of triple star system candidates by cross-matching the table “`nss_two_body_orbit`” in Gaia DR3 with several databases of eclipsing binaries, such as APASS (AAVSO Photometric All Sky Survey: Munari et al. 2014), ASAS-SN (All-Sky Automated Survey for Supernovae: Shappee et al. 2014; Rowan et al. 2022), GCVS (General Catalog of Variable Stars: Samus’ et al. 2017), Kepler (Kepler Eclipsing Binary Stars: Kirk et al. 2016), TESS (TESS Eclipsing Binary Stars: Prša et al. 2022), and VSX (The International Variable Star Index: Watson et al. 2006). However, Czavalinga et al. (2023) have not included G1010 in the list of the triple star system candidates. This is because G1010 is not listed in these database. Bashi & Tokovinin (2024) have also made a candidate list of triple star systems from binaries with astrometric solutions in Gaia DR3, or binaries categorized into `Orbital` and `AstroSpectroSB1` by a data type `nss_solution_type`. Because G1010 has only a spectroscopic solution in Gaia DR3 (or categorized into SB1), G1010 is absent in the list.

Prša et al. (2022) have stated that it is difficult for TESS to find eclipsing binaries with orbital periods of  $\gtrsim 13$  days due to its duty cycle. That should be the reason why TESS Eclipsing Binary Stars do not include G1010 as an eclipsing binary as described above. We can identify G1010 as an eclipsing binary, because we concentrate G1010, and know in advance that G1010 is a triple star system.

Figure 8 shows the relation between inner and outer binary periods in triple star system candidates compiled by Czavalinga et al. (2023) based on Gaia DR3 and TESS. The star sign indicates G1010. We indicate a line of  $P_{\text{out}}/P_{\text{in}} = 5$ , above which triple star systems are dynamically stable (Mardling & Aarseth 2001). We note amplitudes of eclipse time variations due to the light-travel time effect and secular effect as  $A_{\text{LTTE}}$  and  $A_{\text{dyn}}$ , respectively (e.g., Borkovits et al. 2015). The amplitude of the light-travel time effect is expressed as

$$\left( \frac{A_{\text{LTTE}}}{\text{day}} \right) \sim 1.1 \times 10^{-4} \left[ \frac{g_m}{M_\odot} \right]^{1/3} \left( \frac{P_{\text{out}}}{\text{day}} \right)^{2/3} \times \sqrt{1 - e_{\text{out}}^2 \cos^2 \omega_1}, \quad (10)$$

where

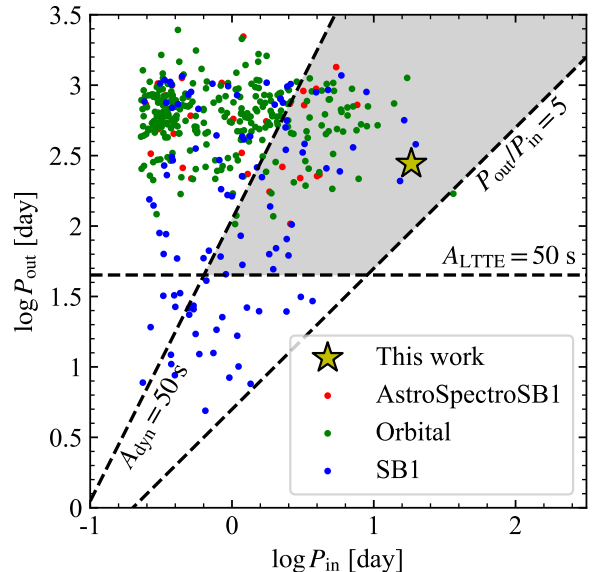


**Fig. 8.** Relation between inner and outer orbital periods of G1010 and triple star system candidates Czavalinga et al. (2023). The star sign indicates G1010. Dots show the triple star system candidates, and their color codes are linked with Gaia NSS orbital solutions. The dashed lines indicate  $P_{\text{out}}/P_{\text{in}} = 5$ ,  $A_{\text{LTTE}} = 50$  s, and  $A_{\text{dyn}} = 50$  s. When we calculate  $A_{\text{LTTE}}$  and  $A_{\text{dyn}}$ , we set  $m_1 = m_2 = m_3 = 1 M_\odot$ ,  $e_{\text{out}} = 0.35$ ,  $i_{\text{out}} = 60$  degrees, and  $\omega_1 = 90$  degrees. The shaded region indicates dynamically stable triple star systems which are easy to be discovered by the analysis of eclipse time variations (Borkovits et al. 2016).

$$g_m = \frac{m_1^3}{(m_1 + m_2 + m_3)^2} \sin^3 i_{\text{out}}. \quad (11)$$

Note that Eq. (11) is similar to Eq. (2), however masses in numerators are different. The amplitude of the secular effect is given by

$$A_{\text{dyn}} = \frac{1}{2\pi} \frac{m_1}{m_1 + m_2 + m_3} \frac{P_{\text{in}}^2}{P_{\text{out}}} (1 - e_{\text{out}}^2)^{3/2}. \quad (12)$$

The shaded region indicates dynamically stable triple star systems which are easy to be discovered by the analysis of eclipse time variations (Borkovits et al. 2016). Although G1010 is located in the shaded region, we find G1010 not by the analysis of eclipse time variations. We recognize that G1010 is a triple star system before finding their eclipses. We use their eclipses solely to determine the inner binary orbit. This means that we can find triple star systems without eclipse time variations, combining low- and high-SNR spectroscopic observations with Gaia DR3. Note that we will determine inner orbits of triple systems without eclipses unlike G1010, if we will perform high SNR spectroscopy like our HDS observation several times.

We can see in Figure 8 that G1010 has a small outer-to-inner period ratio ( $\sim 15$ ), compared with triple star system candidates from Gaia DR3 (Czavalinga et al. 2023). This is true when we compare G1010 with triple star systems discovered from the Kepler field (Borkovits et al. 2016; 2025b). As for the outer eccentricity, inner binary mass, and mass ratio of the primary star to the inner binary, G1010 is similar to triple star systems found with eclipse time variations by Borkovits et al. (2025b).

## 9 Conclusions

We discover a triple star system G1010, while searching for compact binaries. We perform follow-up spectroscopic observations several times with GAOES-RV, MALLS, and HDS, determine its outer orbit by RV variation, and find the outer orbital period and eccentricity of  $\sim 277.2$  days and  $\sim 0.230$ , respectively. We detect an inner binary in G1010 with the SB3 spectral fit for a high-SNR spectroscopic observation performed by Subaru HDS. We adopt the isochrone fitting, and estimate the primary, secondary, and tertiary masses of  $\sim 0.85$ ,  $\sim 0.63$ , and  $\sim 0.61 M_{\odot}$ , respectively. The inner orbit has the orbital period of  $\sim 18.3$  days, and a small orbital eccentricity ( $\sim 0.01$ ), according to the combination of our findings and the TESS data. Although G1010 has a relatively small outer-to-inner period ratio ( $\sim 15$ ), compared with triple star systems discovered before, the other parameters are typical for triple star systems.

In the last decade and a half, triple star systems like G1010 have been discovered via eclipse time variations. On the other hand, we find G1010 without adopting eclipse time variation. We only use eclipses in order to determine the inner orbit of G1010. We recognize the presence of the inner binary before finding these eclipses. For G1010, we can determine the inner orbit by analyzing these eclipses fortunately. Even unless G1010 indicated eclipses, we could determine its inner orbit, performing high-SNR spectroscopic observations several times. Our discovery implies the possibility that we can find triple star systems without eclipse time variations, combining low- and high-SNR spectroscopic observations with Gaia DR3, and the upcoming Gaia DR4. Especially, such triple star systems will be found in the course of searching for compact binaries like our survey.

Finally, we emphasize that a high-SNR ( $\gtrsim 200$  per pixel) spectroscopic observation with a 10-m class telescope is mandatory for

this discovery. Since the mass ratio of each inner binary component to the primary star is small ( $\sim 0.7$ ), absorption lines of each binary component cannot be identified by a low-SNR ( $\gtrsim 20$  per pixel) spectroscopic observation. Moreover, a triple star system is rare, in other words, distant and faint. We need to use a 10-m class telescope, such as the Subaru telescope, in order to achieve high SNR within reasonable time.

## Acknowledgments

This research is based on data collected at the 3.8-m Seimei telescope at the Okayama observatory, the 2-m NAYUTA telescope at the Nishi-Harima Astronomical Observatory (NHAO), and the Subaru Telescope. The 3.8-m Seimei telescope is operated by the National Astronomical Observatory of Japan, and Kyoto University. We are grateful to all the staff members at the Okayama observatory for their help during the observations. NHAO is operated by Center for Astronomy at University of Hyogo. We would like to express our gratitude to all the staff members at NHAO for their support during the observations. The Subaru telescope is operated by the National Astronomical Observatory of Japan. We are honored and grateful for the opportunity of observing the Universe from Maunakea, which has the cultural, historical, and natural significance in Hawaii.

The GAOES-RV project started as a collaboration between Gunma Astronomical Observatory and Institute of Science Tokyo. Based on the contract signed between the two parties, GAOES-RV is lent to Institute of Science Tokyo and operated at the Seimei Telescope.

This work presents results from the European Space Agency (ESA) space mission Gaia. Gaia data are being processed by the Gaia Data Processing and Analysis Consortium (DPAC). Funding for the DPAC is provided by national institutions, in particular the institutions participating in the Gaia MultiLateral Agreement (MLA). The Gaia mission website is <https://www.cosmos.esa.int/gaia>. The Gaia archive website is <https://archives.esac.esa.int/gaia>.

This research has made use of the VizieR catalogue access tool, CDS, Strasbourg, France (Ochsenbein 1996). The original description of the VizieR service was published in Ochsenbein et al. (2000). This research has used data, tools or materials developed as part of the EXPLORE project that has received funding from the European Union’s Horizon 2020 research and innovation programme under grant agreement No 101004214.

We acknowledge the use of TESS High Level Science Products (HLSP) produced by the Quick-Look Pipeline (QLP) at the TESS Science Office at MIT, which are publicly available from the Mikulski Archive for Space Telescopes (MAST). Funding for the TESS mission is provided by NASA’s Science Mission directorate.

## Funding

This research was supported by Grants-in-Aid for Scientific Research, 24K07040 and 25K01035 (A.T.) from the Japan Society for the Promotion of Science.

## Data availability

The data underlying this article are available publicly.

## References

Abbott, B. P., Abbott, R., Abbott, T. D., et al. 2017, *ApJL*, 848, L12

Abbott, R., Abbott, T. D., Acernese, F., et al. 2023, *Physical Review X*, 13, 041039

Baran, A. S., Zola, S., Blokesz, A., Østensen, R. H., & Silvotti, R. 2015, *A&A*, 577, A146

Bashi, D., & Tokovinin, A. 2024, *A&A*, 692, A247

Bingham, E., Chen, J. P., Jankowiak, M., et al. 2018, arXiv preprint arXiv:1810.09538

Borkovits, T., Hajdu, T., Sztakovics, J., et al. 2016, *MNRAS*, 455, 4136

Borkovits, T., Rappaport, S., Hajdu, T., & Sztakovics, J. 2015, *MNRAS*, 448, 946

Borkovits, T., Rappaport, S. A., Hajdu, T., et al. 2020, *MNRAS*, 493, 5005

Borkovits, T., Derekas, A., Kiss, L. L., et al. 2013, *MNRAS*, 428, 1656

Borkovits, T., Rappaport, S. A., Mitnyan, T., et al. 2025a, arXiv e-prints, arXiv:2510.04565

—. 2025b, *A&A*, 695, A209

Cardelli, J. A., Clayton, G. C., & Mathis, J. S. 1989, *ApJ*, 345, 245

Castelli, F., & Kurucz, R. L. 2003, in *IAU Symposium*, Vol. 210, *Modelling of Stellar Atmospheres*, ed. N. Piskunov, W. W. Weiss, & D. F. Gray, A20

Chakrabarti, S., Simon, J. D., Craig, P. A., et al. 2023, *AJ*, 166, 6

Choi, J., Dotter, A., Conroy, C., et al. 2016, *ApJ*, 823, 102

Coelho, P., Barbay, B., Meléndez, J., Schiavon, R. P., & Castilho, B. V. 2005, *A&A*, 443, 735

Conroy, K. E., Prša, A., Stassun, K. G., et al. 2014, *AJ*, 147, 45

Czavala, D. R., Borkovits, T., Mitnyan, T., Rappaport, S. A., & Pál, A. 2023, *MNRAS*, 526, 2830

Ding, X., Ji, K., Song, Z., et al. 2024, *AJ*, 168, 217

Dotter, A. 2016, *ApJS*, 222, 8

Eisner, N. L., Johnston, C., Toonen, S., et al. 2022, *MNRAS*, 511, 4710

El-Badry, K. 2024a, *New Astronomy Reviews*, 98, 101694

—. 2024b, *The Open Journal of Astrophysics*, 7, 38

—. 2025, *The Open Journal of Astrophysics*, 8, 62

El-Badry, K., Rix, H.-W., Cendes, Y., et al. 2023a, *MNRAS*, 521, 4323

El-Badry, K., Rix, H.-W., Quataert, E., et al. 2023b, *MNRAS*, 518, 1057

El-Badry, K., Rix, H.-W., Latham, D. W., et al. 2024, *The Open Journal of Astrophysics*, 7, 58

Foreman-Mackey, D., Hogg, D. W., Lang, D., & Goodman, J. 2013, *PASP*, 125, 306

Fouesneau, M. 2025, *pyphot*, doi:10.5281/zenodo.14712174

Gaia Collaboration, Arenou, F., Babusiaux, C., et al. 2023a, *A&A*, 674, A34

Gaia Collaboration, Montegriffo, P., Bellazzini, M., et al. 2023b, *A&A*, 674, A33

Gaia Collaboration, Panuzzo, P., Mazeh, T., et al. 2024, *A&A*, 686, L2

Gaulme, P., Borkovits, T., Appourchaux, T., et al. 2022, *A&A*, 668, A173

Geier, S., Dorsch, M., Dawson, H., et al. 2023, *A&A*, 677, A11

Gelman, A., Carlin, J. B., Stern, H. S., et al. 2014, *Bayesian data analysis*, 3rd edn., *Texts in statistical science* (CRC Press)

Gies, D. R., Matson, R. A., Guo, Z., et al. 2015, *AJ*, 150, 178

Gies, D. R., Williams, S. J., Matson, R. A., et al. 2012, *AJ*, 143, 137

Grevesse, N., & Sauval, A. J. 1998, *Space Sci. Rev.*, 85, 161

Hajdu, T., Borkovits, T., Forgács-Dajka, E., Sztakovics, J., & Bódi, A. 2022, *MNRAS*, 509, 246

Hajdu, T., Borkovits, T., Forgács-Dajka, E., et al. 2019, *MNRAS*, 485, 2562

Hoffman, M. D., & Gelman, A. 2011, arXiv e-prints, arXiv:1111.4246

Iben, Jr., I., & Tutukov, A. V. 1984, *ApJS*, 54, 335

Kipping, D. M. 2013, *MNRAS*, 435, 2152

Kirk, B., Conroy, K., Prša, A., et al. 2016, *AJ*, 151, 68

Kostov, V. B., Rappaport, S. A., Borkovits, T., et al. 2024, *ApJ*, 974, 25

Kostov, V. B., Powell, B. P., Rappaport, S. A., et al. 2026, *AJ*, 171, 29

Kurucz, R. L., & Bell, B. 1995, *Atomic line list*

Lalement, R., Vergely, J. L., Babusiaux, C., & Cox, N. L. J. 2022, *A&A*, 661, A147

Lee, J. W., Hong, K., & Hinse, T. C. 2015, *AJ*, 149, 93

Lee, J. W., Kim, S.-L., Hong, K., Lee, C.-U., & Koo, J.-R. 2014, *AJ*, 148, 37

Lee, J. W., Kim, S.-L., Lee, C.-U., et al. 2013, *ApJ*, 763, 74

Lejeune, T., Cuisinier, F., & Buser, R. 1997, *A&AS*, 125, 229

—. 1998, *A&AS*, 130, 65

Li, X., Wang, S., Zhao, X., et al. 2022, *ApJ*, 938, 78

Mardling, R. A., & Aarseth, S. J. 2001, *MNRAS*, 321, 398

Martin, D. C., Fanson, J., Schiminovich, D., et al. 2005, *ApJL*, 619, L1

Masuda, K. 2022, *ApJ*, 937, 94

Mazeh, T., Faigler, S., Bashi, D., et al. 2022, *MNRAS*, 517, 4005

Mitnyan, T., Borkovits, T., Czavala, D. R., et al. 2024, *A&A*, 685, A43

Mitnyan, T., Borkovits, T., Rappaport, S. A., Pál, A., & Maxted, P. F. L. 2020, *MNRAS*, 498, 6034

Moharana, A., Helminiak, K. G., Marcadon, F., et al. 2023, *MNRAS*, 521, 1908

—. 2024, *A&A*, 690, A153

Munari, U., Henden, A., Frigo, A., et al. 2014, *AJ*, 148, 81

Nagarajan, P., El-Badry, K., Triaud, A. H. M. J., et al. 2024, *PASP*, 136, 014202

Ochsenbein, F. 1996, *The VizieR database of astronomical catalogues*, doi:10.26093/CDS/VIZIER

Ochsenbein, F., Bauer, P., & Marcout, J. 2000, *A&AS*, 143, 23

Padmanabhan, N., Schlegel, D. J., Finkbeiner, D. P., et al. 2008, *ApJ*, 674, 1217

Paxton, B., Bildsten, L., Dotter, A., et al. 2011, *ApJS*, 192, 35

Paxton, B., Cantiello, M., Arras, P., et al. 2013, *ApJS*, 208, 4

Paxton, B., Marchant, P., Schwab, J., et al. 2015, *ApJS*, 220, 15

Phan, D., Pradhan, N., & Jankowiak, M. 2019, arXiv preprint arXiv:1912.11554

Prša, A., Kochoska, A., Conroy, K. E., et al. 2022, *ApJS*, 258, 16

Qi, S., Gu, W.-M., Yi, T., et al. 2023, *AJ*, 165, 187

Rappaport, S., Deck, K., Levine, A., et al. 2013, *ApJ*, 768, 33

Rappaport, S. A., Borkovits, T., Gagliano, R., et al. 2022, *MNRAS*, 513, 4341

Rappaport, S. A., Borkovits, T., Mitnyan, T., et al. 2024, *A&A*, 686, A27

Ricker, G. R., Winn, J. N., Vanderspek, R., et al. 2015, *Journal of Astronomical Telescopes, Instruments, and Systems*, 1, 014003

Rocha, D. F., Emilio, M., Labadie-Bartz, J., et al. 2025, arXiv e-prints, arXiv:2511.05761

Rowan, D. M., Jayasinghe, T., Stanek, K. Z., et al. 2022, *MNRAS*, 517, 2190

Rowan, D. M., Jayasinghe, T., Tucker, M. A., et al. 2024, *MNRAS*, 529, 587

Samus', N. N., Kazarovets, E. V., Durlevich, O. V., Kireeva, N. N., & Pastukhova, E. N. 2017, *Astronomy Reports*, 61, 80

Sato, B., Hashimoto, O., Omiya, M., et al. 2024, in *Society of Photo-Optical Instrumentation Engineers (SPIE) Conference Series*, Vol. 13096, *Ground-based and Airborne Instrumentation for Astronomy X*, ed. J. J. Bryant, K. Motohara, & J. R. D. Vernet, 1309644

Shappee, B. J., Prieto, J. L., Grupe, D., et al. 2014, *ApJ*, 788, 48

Shenar, T., Sana, H., Mahy, L., et al. 2022, *Nature Astronomy*, 6, 1085

Shiraishi, Y., Hotokezaka, K., Masuda, K., et al. 2025, arXiv e-prints, arXiv:2509.12808

Skrutskie, M. F., Cutri, R. M., Stiening, R., et al. 2006, *AJ*, 131, 1163

Steffen, J. H., Quinn, S. N., Borucki, W. J., et al. 2011, *MNRAS*, 417, L31

Tanikawa, A., Hattori, K., Kawanaka, N., et al. 2023, *ApJ*, 946, 79

Tanikawa, A., Wang, L., Fujii, M. S., et al. 2025, *The Open Journal of Astrophysics*, 8, 79

Tokovinin, A. 2014a, *AJ*, 147, 86

—. 2014b, *AJ*, 147, 87

—. 2018, *ApJS*, 235, 6

Tomoyoshi, M., Masuda, K., Hirano, T., et al. 2024, *ApJ*, 977, 151

Tucker, M. A., Wheeler, A. J., Rowan, D. M., & Huber, M. E. 2025, *The Open Journal of Astrophysics*, 8, 61

Valenti, J. A., & Fischer, D. A. 2005, *ApJS*, 159, 141

Vergely, J. L., Lallement, R., & Cox, N. L. J. 2022, *A&A*, 664, A174

Watson, C. L., Henden, A. A., & Price, A. 2006, *Society for Astronomical Sciences Annual Symposium*, 25, 47

Webbink, R. F. 1984, *ApJ*, 277, 355

Wright, E. L., Eisenhardt, P. R. M., Mainzer, A. K., et al. 2010, *AJ*, 140, 1868

Yamaguchi, N., El-Badry, K., Rees, N. R., et al. 2024a, *PASP*, 136, 084202

Yamaguchi, N., El-Badry, K., Fuller, J., et al. 2024b, *MNRAS*, 527, 11719

Yang, Y., Michel, R., Yuan, H., Wang, S., & Tamayo, F. 2023, *MNRAS*, 522,

3076

Yenawine, M. E., Welsh, W. F., Orosz, J. A., et al. 2022, *ApJ*, 924, 66  
Yi, T., Gu, W.-M., Zhang, Z.-X., et al. 2022, *Nature Astronomy*, 6, 1203  
Yuan, H., Wang, S., Bai, Z., et al. 2022, *ApJ*, 940, 165  
Zasche, P., Wolf, M., Kučáková, H., et al. 2015, *AJ*, 149, 197  
Zhang, Z.-X., Liu, H.-B., Yi, T., Sun, M., & Gu, W.-M. 2024, *ApJL*, 961, L48  
Zhao, X., Mu, H., Wang, S., et al. 2024, *ApJ*, 964, 101  
Zheng, L.-L., Gu, W.-M., Sun, M., et al. 2022, *ApJ*, 936, 33  
Zheng, L.-L., Sun, M., Gu, W.-M., et al. 2023, *Science China Physics, Mechanics, and Astronomy*, 66, 129512  
Zhu, H., Wang, W., Li, X., Li, J.-j., & Tian, P. 2025, *Journal of High Energy Astrophysics*, 45, 428